## Research Highlights

- A low-rise wood building was constructed and equipped with state-of-the-art pressure and force monitoring equipment.
- The building was exposed to real wind events and wind, pressure and force data were collected.
- In addition to the full-scale building, a model of the test building was constructed and tested in a boundary layer wind tunnel and a finite element model was developed and analyzed.
- Field data were used to verify the simulation approaches. Most importantly, for very first time, wind-induced loads were captured at various key points and provided valuable information regarding the wind load paths.

# Wind load transfer mechanisms on a low wood building using full-scale load data

Ioannis Zisis*, Ted Stathopoulos

*Department of Building, Civil and Environmental Engineering, Concordia University, Montreal, Quebec, Canada*

**Corresponding Author: i_zisis@live.concordia.ca*

## Abstract

The wind-induced response of low-rise wood buildings has been evaluated by monitoring a specially instrumented test building exposed to real wind action. The field facilities included a state-of-the-art data acquisition system which collected wind, pressure and force data. In addition to the field monitoring, a 1:200 scaled model of the test building was tested in the wind tunnel and the envelope wind pressures were estimated for various terrain exposures. The wind-induced pressures obtained from both the full-scale and wind tunnel experiments were incorporated in the finite element model of the test building and its response was numerically derived.

Vast amounts of experimental data were generated during the long-term monitoring of the test building. These data were used to successfully verify the simulation approaches in terms of both wind-induced pressures and structural forces. Some limited discrepancies were observed in the peak pressure coefficients for locations close to the roof ridge and corners. The field acquired force data revealed that the majority of the wind uplift force is supported by the two side walls. Moreover, it was experimentally verified that the wind-induced load was attenuated as it was transferred through the buildings' structural system. This attenuation was estimated to be at least 17%, as far as the total foundation uplift force is concerned, and reached the 28% for certain approaching wind directions.

**Keywords**: Wind load paths, structural attenuation, field monitoring, wind tunnel tests, structural performance.

# 1 Introduction

Wind-induced natural disasters have been frequently reported as some of the most fatal and costly catastrophes during the past few decades. Several regions across the globe have been afflicted by extreme wind phenomena causing severe damage to residential and other construction. The aftermath of recent wind-related catastrophes revealed a significant amount of casualties. Of particular intensity was the disastrous effect on low-rise residential properties that suffered in several cases from a complete damage.

Numerous studies have been carried out focusing on the estimation of wind-induced envelope pressures using in most cases wind tunnel experimental techniques and less often full-scale studies. The first full-scale experimental efforts were performed in the field and, amongst others, included the Aylesbury study (Eaton and Mayne 1975), the Texas Tech University projects - also known as Wind Engineering Research Field Laboratory – (Kim and Mehta 1977, Levitan and Mehta 1992a and 1992b) and the Silsoe Structures project (Robertson and Glass 1988). Most recent experimental efforts have been carried out on either full- or large-scale structures in a laboratory environment. The fundamental difference of this experimental approach to the field studies is the fact that wind action is replicated by either an array of large fans (Leatherman et al. 2007, Datin 2010) or specially designed pressure actuators (Bartlett et al. 2007, Kopp et al. 2010). A more detailed discussion regarding the various full-scale studies has been presented by Zisis (2011).

A key component that has not yet been investigated adequately is the flow of wind-induced forces through the structural system and their attenuation due to dynamic and other structural aspects of light frame construction. The main reason of lack of such studies is that they require

field monitoring with heavily instrumented full-scale facilities or special costly laboratory accommodations.

## 2 Project description

### *2.1 Load Path in Wood Buildings*

A collaborative research project dealing with load paths in wood buildings was carried out to assess the application of environmental loads and their actual transferring through the building elements from the envelope to the foundation. Several experimental approaches were implemented in this study with most important the structural monitoring of a light-frame wood structure subjected to high wind loads (Doudak 2005; Zisis and Stathopoulos 2009; Zisis et al. 2011).

### *2.2 Facilities*

The field facilities include a tower with three anemometers and a single-storey test building constructed according to the needs of the particular research project. The external dimensions of the structure are 8.6m by 17.2m and the roof height is 5.6m. The test building is equipped with 40 pressure taps, 12 of them on the wall and 28 on the roof, as shown in Fig. 1a. The roof pressure taps were distributed in three main frames and were equally spaced from each other. The load cell system is an innovative part of this study. A total number of six 1-D load cells were placed between the wall and the roof and twenty-seven 3-D load cells were also installed around the perimeter of the building at the wall-to-foundation interface. The location of the load cells is shown in Fig. 1b. It should be mentioned that the building is completely isolated from the foundation and the only points of contact are the 3-D load cells. This construction detail assures the transfer of the applied load to the foundation only through the load cells. North is the reference zero for all wind direction measurements. The ridge of the gable roof is oriented at 43

degrees from North, i.e. roughly on the Northeast - Southwest line. The notation of all sensors and house components (e.g. walls, roof etc) is provided with respect to the building orientation (Fig. 2). Additional details about earlier construction stages of the experimental facilities as well as specifications of the instrumentation can be found in Doudak (2005) and Zisis (2011).

### *2.3 Wind tunnel experiments*

A scaled model of the study building was tested in the Building Aerodynamics Laboratory at Concordia University. The model was of 1:200 geometric scale and was equipped with 126 pressure taps located on wall and roof surfaces. The wind tunnel model was tested for thirty-six angles of attack and for three different upstream exposures i.e. open, light suburban and heavy suburban terrains. The power law exponents for those simulated exposures were 0.16, 0.22, and 0.28 respectively and the turbulence intensities at ridge height were 17.9%, 20.2% and 26.4% respectively (Table 1). The pressure traces for the various taps and upstream terrain configurations were captured using a highly sensitive system of pressure transducers. Wind tunnel observations yielded a detailed picture of wind-induced pressures applied on the building envelope.

## 3 Results

### *3.1 Verification of experimental facilities and methods*

The test building is resting on top of the 27 foundation load cells. As previously described, there is no other point of contact between the foundation wall and the superstructure besides these load cells. To verify their accuracy and performance a series of controlled tests were carried out. More specifically, the test building was subjected to a static ramp load using an external loader. The point of application was at the top of the wall close to the wall-to-roof

intersection. The applied load was monitored by using a “pancake” type tension/compression load cell connected to the main data acquisition system. The load level was increased periodically using intervals of approximately 60 seconds and a load step of 1 kN. The notation used for the tests comprised by the frame number and the orientation of the wall that the load is applied to. For example, for static load test FR14-NW the point of application is on the 14$^{th}$ frame of the North-West wall. The results are presented in Fig. 3. The maximum load applied was determined based on the shear wall capacity (i.e. non-destructive maximum deflection) on the direction tested and was ranging between 1.5 and 8.0 kN.

The tests performed on the North-West (e.g. Fig. 3a) and South-East walls show excellent agreement between the externally applied and the recorded by the load cells total foundation load. It should be mentioned that the measured (by the load cells) load is fluctuating, as it includes a wind-induced load component. Despite the efforts to conduct the static load tests during relatively calm wind periods, the duration of each test made it almost impossible to exclude some wind gust effects from the load monitoring. Two additional tests were performed in the longitudinal direction which allowed reaching higher load levels. As it can be seen in Fig. 3b (North-East wall), the agreement between the applied load and that recorded by the load cells is excellent for lower stress levels. The two signals diverge when the applied load exceeds the 4-5 kN level, which indicates a possible unlocking of some internal stresses (e.g. temperature deformations). Another possibility could be a contact point at the foundation level during large diaphragmatic deformations. In any case, the particular phenomenon occurs for significantly high structural system deformations, which could only be generated by very high intensity winds.

The field monitoring produced a vast amount of data which, as a result, made their handling and interpretation a time consuming and computationally demanding process. The primary filtering criterion applied to the available records was the stationarity verification. The identification was performed in two phases, namely Phase I which includes the preliminary visual and moving average slope inspections, and Phase II which includes the RUN and TREND tests. Furthermore, these verifications were performed for the mean and mean square values of both wind speed and wind direction. Due to the large number of available records an analytical routine was developed to divide longer traces into 10-minute duration segments and estimate their linear moving average slope. Then the qualified segments were inspected visually for abnormalities or sudden instabilities (e.g. spikes, steps etc).

The second and more detailed phase of stationarity verification was conducted to the visually inspected and PHASE I qualified records by using the RUN and TREND tests. Both tests were applied to a sequence of independent sample measurements, i.e. wind speed and direction, for both mean and mean square values. Special attention was paid to properly identify the interval length and assure independence of the sequential data. The process described by Levitan (1988) has been implemented to identify the interval length based on the field observations. Several representative wind speed and direction records have been selected and used to plot the variation of the autocorrelation function with respect to time. Two representative plots are presented in Fig. 4 and include wind speed and direction for records acquired during May 2009. As the plots indicate the time lag should be at least 25 seconds to assure independence between the samples used in both RUN and TREND tests.

The PHASE I selection resulted in 163 qualified records, out of which 41 were acquired in 2008 and 122 in 2009. These 163 qualified records were then considered for the RUN and

TREND tests. The confidence level for both tests was 95% and three time lag cases were examined, i.e. 30, 40 and 50 seconds time lag. The first case resulted in 87 stationary records (Fig. 5), the second case in 93 stationary records and the last one in 106 stationary records. After considering the autocorrelation function of several records, the records of the 30 seconds time lag were selected for further analysis. It should be noted that only a limited number of these records were acquired with the pressure taps open, i.e. no precipitation was expected therefore the taps were not protected. These records were used for both pressure and load data interpretation whereas the rest of the stationary records were considered for load and wind data analysis.

### *3.2 Local wind pressure coefficients*

The verification of the wind tunnel simulation experiments was performed in terms of dimension-less mean and peak pressure coefficients defined as:

$$c_{p,mean/peak} = \frac{p_{mean/peak} - p_a}{1/2\rho\overline{V_{r.h.}}^2} \quad (1)$$

where $\rho$=air density (kg/m$^3$); $V_{r.h.}$: mean wind speed at roof height (m/s); $p_a$=ambient atmospheric pressure (Pa), $p_{mean}$=mean surface pressure (Pa) and $p_{peak}$=peak surface pressure (Pa). It should be noted that for the full-scale calculations the mean values where based on a 10-minute average and the instantaneous peak on a 3-second average (full-scale time scale). A representative stationary full-scale record was selected (May 25$^{th}$, 2009) and the comparison was made for all pressure taps located on Frame 14 (see Fig. 1). The results are presented in Fig. 6a (mean pressure coefficients) and Fig. 6b (peak pressure coefficients). The average wind direction for the specific record was 326 degrees (see Fig. 2) therefore the case of 330 degrees from the wind tunnel experiments was selected for comparison. It should be noted, that after analyzing wind speed and direction data from the weather station it was concluded that the majority of the

dominant direction records (i.e. South-West to North-West) correspond to heavy suburban terrain (see Zisis et al. 2011 and Zisis 2011). For the mean pressure coefficients the field values show an excellent agreement to the wind tunnel results (heavy suburban terrain; i.e. $\alpha$=0.28). The agreement for most of the pressure taps remains exceptional even for the peak pressure coefficients. The small discrepancies occurring for the close to the ridge roof and the two wall pressure taps can be attributed to the higher standard deviation of the field wind direction.

In addition to the frame pressure tap comparisons, the wind tunnel tests were verified by comparing mean and peak pressure coefficients from all wall and roof pressure taps. As was presented and discussed in the previous comparisons, some of the discrepancies between the field and wind tunnel pressure coefficients were attributed to the fluctuations of the wind direction in the 10-minute full-scale records. More specifically, the wind tunnel tests were conducted at thirty-six distinct wind angles of attack whereas field records were characterized by high variability in wind direction even during shorter periods of time. To account for these directional fluctuations the field mean and peak pressure coefficients from 10-minute records were compared to a range of wind tunnel directions (with ± 20 degrees of any nominal direction - which is close to the standard deviation of the wind direction in most field records). Therefore, for this analysis a single full-scale record was compared to five different wind tunnel cases and this process was repeated for each of the forty pressure taps. The final scatter plot, for all 40 pressure taps, was formed only with the results corresponding to the wind direction that seemed to be predominant through each individual comparison.

A representative comparison is presented in Fig. 7, in which a 10-minute record from May 21$^{st}$, 2009 is compared to the wind tunnel results. For the specific record, the mean wind speed at 10 meters height was 28.0 km/h and the mean wind direction at the same height was 259.4

degrees with a standard deviation equal to 14.9 degrees. Considering the mean wind direction of approximately 260 degrees the full-scale mean and peak pressure coefficients were compared to the wind tunnel results for the range of 240 to 280 degrees. By following this approach the agreement between the two experimental results is significantly improved. As the graph clearly shows, positive and negative peak values compare quite well with only few outliers from the generally tight correlation between field and wind tunnel pressure coefficients. The coefficients of determination ($R^2$) are equal to 0.99, 0.92 and 1.00 for the cases of the mean, minimum and maximum pressure coefficients respectively. The agreement is particularly good even for the extreme peak values, such as the absolute minimum and maximum pressure coefficients, which for the specific record reach the values of -4.7 and +2.7 respectively.

### *3.3 Wind uplift forces*

#### *3.3.1 Wind load paths*

The main interest in this study was to examine how the applied wind load is transferred from the building envelope down to the foundation level. The availability of both roof and foundation load cells provided the appropriate data to perform several comparisons and identify similarities between internal loads at different locations, as well as transfer patterns for wind-induced forces.

The comparisons presented in Fig. 8, are related to the correlation between the force monitored at a single roof load cell and that recorded at different locations at the foundation level. A 10-minute record was selected (June 1$^{st}$, 2009) and the load from roof load cell $L_{NW\text{-}R,2}$ was compared to various foundation loads. For the specific record, the 10-minute mean wind speed at the roof height was 26.9 km/h and the mean wind direction was 313 degrees. The first comparison was made with the foundation load cell $L_{NW\text{-}4}$ located immediately below the specific roof load cell and supporting the same frame in which $L_{NW\text{-}R,2}$ is part of (i.e. Frame 14 –

see Fig. 1). The scatter plot of the two 10-minute force traces is shown in Fig. 8a. The correlation between them is significantly high, with the square of the linear correlation coefficient reaching the value of 0.95. In addition to the comparison to a single foundation load cell, traces of the total load recorded by the two foundation side-walls (North-West and South-East walls) were compared to that from the roof load cell ($L_{NW\text{-}R,2}$). The trace used for each wall was the sum of its foundation load cells. As it can be seen in Fig. 8b and 8c, the correlation of the traces is weaker as the load travels farther. The North-West wall, located below the roof load cell, showed the highest coefficient of determination ($R^2$=0.60) whereas the comparison to the SW wall resulted into a value of 0.38. This wall is located on the opposite side of where the roof load cell is located which is also the leeward side of the building for the considered 10-minute record. Similar results were acquired when the opposite roof load cell of Frame 14 ($L_{SE\text{-}R,2}$) was considered. The correlation between the particular roof load cell and the foundation load cell $L_{SE\text{-}5}$, which is located directly below it, was higher compared to the cases of the two foundation sidewalls. As Fig. 8d-f indicate, the coefficients of determination were found to be equal to 0.96, 0.90 and 0.55 for the cases of the single foundation load cell, the South-East and North-West foundation walls respectively.

The correlation of the load transferred to the four foundation walls was examined by comparing the ratios of instantaneous force coefficients defined as:

$$c_{f,i} = \frac{F_i}{(1/2\rho\overline{V_{r.h.}}^2)A} \tag{2}$$

where ρ=air density (kg/m$^3$); $V_{r.h.}$: mean wind speed at roof height (m/s); $F_i$=load cell(s) force reading (N), and A=building area (m$^2$). More specifically, load data acquired from the twenty-seven foundation load cells were grouped in four sets, each corresponding to an individual foundation wall (see Fig. 2), and normalized by the instantaneous dynamic pressure and the area

of the test building in order to get dimensionless force coefficients. These data were also sorted with respect to the wind direction at 10 meters height. The comparison was performed in the form of scatter plots where the distribution and the correlation of various cases were examined.

The results of this analysis are presented in Fig. 9 and were grouped in terms of approaching wind direction ranges (see Fig. 2). More specifically, Fig. 9a to 9d present the cases of incident wind approaching from the North-East (i.e. 13.5 to 66.5 degrees), South-East (i.e. 66.5 to 193.5 degrees), South-West (i.e. 193.5 to 246.5 degrees) and North-West (i.e. 246.5 to 13.5 degrees) respectively. These scatter plots compare the correlation between the two endwalls (i.e. south-east and north-west walls) and the two sidewalls (i.e. north-east and south-west walls). The comparison clearly shows that the contribution of the endwall is minimal compared to that of the sidewalls despite the relatively high coefficient of determination which ranges from 0.53 to 0.78. The ratio between the load transferred to the side walls to that carried by the endwalls, ranges from 2.67 (South-West; 193.5-246.5 degrees) to 3.81 (North-West; 246.5-13.5 degrees).

*3.3.2 Wind-induced structural attenuation*

In order to evaluate the wind-induced load transfer patterns in a more quantitative manner and to account also for the dynamic nature of the wind action, a more comprehensive approach was followed. A 3-D finite element model was created to evaluate the wind-induced internal force flows in the test building. More than 20,000 elements were used to simulate in high detail the structural system of the actual test building including effects of secondary components like rigid insulation and siding layers in exterior walls. Analysis was performed for several load scenarios including the computationally intense cases of the field acquired pressure time histories. The data acquired from the forty pressure taps on the full-scale building were applied as individual time series on forty effective surface areas, and the analysis was performed using the Hilber-Hughes-

Taylor time integration method. Considering the sampling rate of 5 Hz for the field monitoring, a 10-minute record consisted of forty 3000-point time series applied as surface pressures simultaneously on shell elements representing the outer building surface. Using this particular method of analysis it was possible to numerically derive internal force and foundation reaction time histories, which were compared to the data captured by the load cells installed in the test building. More details about the finite element modeling of the test building can be found in Zisis (2011).

Fig. 10 presents representative results, for a stationary 10-minute record, which were acquired on June 4$^{th}$, 2009. The mean wind speed for that record is 14.5 km/h and the mean wind direction 310 degrees at the mean roof height. More specifically, Fig. 10a-b compares force data for Frame 14 (see Fig. 1) at the roof level ($L_{NW\text{-}R,2}$ and $L_{SE\text{-}R,2}$); Fig. 10c-d at the foundation level ($L_{NW,4}$ and $L_{SE,5}$); and Fig. 10e-f the total uplift foundation force $\Sigma\{L_{SE,i}+L_{SW,i}+L_{NE,i}+L_{NW,i}\}$. Fig. 10a, 10c and 10e clearly illustrate good general agreement between the two traces, especially for lower force levels. Importantly however, for most peak values the predicted force exceeds the observed forces captured by the load cells. This behaviour identifies that although the applied load should generate predicted responses at various components, (e.g. roof to wall, wall to foundation interfaces) the actual force monitoring reveals attenuation of peak forces and reactions. The ratios between the load cell and the FEA (finite element model) values range from 0.6 to 0.7 for Frame 14 roof and foundation level and from 0.7 to 0.8 for the total uplift foundation force. It should be noted, that the lower ratios observed in Frame 14 compared to the total foundation uplift force, indicate that a significant portion of the wind load transferred from the envelope to the truss and walls, spreads in the adjacent frames. This effect has the result that FEA predicts higher local loads for Frame 14 whereas in reality the forces captured in the specific frame are

somewhat smaller. The physical explanation for the attenuation of force magnitudes as affects of wind pressures flow from exterior surfaces through the superstructure and into the foundation is believed to be the result of dynamic fluctuation in surface pressures and dynamic (kinetic) force flows with the structural system. Both of those are effects that the finite element model does not incorporate. By implication, it can be expected that wind design practices based on static analysis of structural systems will tend to conservatively estimate true building performances, in the present and other contexts.

Attenuation of internal peak forces is also demonstrated by the scatter plots presented in Fig. 10b, 10d and 10f. Those plots include all 3,000 data points with each corresponding to a 10-minute record. The ratios in this case (unconstrained linear regression analysis) are 0.73, 0.72 and 0.86 for the cases of roof level (Frame 14), foundation level (Frame 14) and total foundation uplift respectively. Constrained coefficients of determination range from 0.78 to 0.86, which indicates cohesive relationships between full-scale and FEA values. The same attenuation effect is demonstrated in Fig. 11, which presents the normalized force spectra of both full scale measured and FEA derived traces. The two spectra compare well for lower frequencies indicating a very similar trend. However, the attenuation effect becomes clear in the higher frequency range depicted by a rapid drop of the full-scale spectra compared to that estimated by finite element analysis. It is also quite interesting that this drop is more dominant in the cases of foundation forces (Fig. 11b and 11c), whereas in the case of the roof force spectra (Fig. 11a) the departure of the full-scale curve is shifted towards the higher frequency region. It should be noted that similar findings have been reported by Robertson et al. (1998) when the wind-induced response of a free-standing wall was estimated using both pressure transducers and load cells. The authors of that study indicated that the higher energy depicted by the pressure based finite

element analysis may be related to the sensitivity of higher envelope suctions to sudden wind direction changes which when uncorrelated result to lower intensity base reactions.

In order to estimate the degree of attenuation in the available full-scale records, the variation of the FEA to full-scale force ratio was examined for higher magnitude wind-induced forces. Therefore, out of the 3000 points assembling each record the first 300 peaks (10% of the sample) were isolated and the ratio of the FEA to full-scale uplift force was calculated. The average value of these peaks was then calculated for several averaging sets, starting from 5 (i.e. the average of the first five ratios) up to 300 (i.e. the average of all 300 ratios). The results of this analysis are presented in Fig. 12, which shows that the ratios of the peak values converge between the 100 and 150 points and the attenuation factor takes values between 0.73 to 0.83 (ratios range from 1.20 to 1.37 with a standard error of 0.018). Fig. 12 also presents the descriptive statistics of the converged ratios when the average of the 300 values is considered. Considering these average ratios, the reduction is estimated to 17% to 27%; i.e. at least 17% of the numerically estimated uplift peak force was not detected by the foundation load cells. Indeed the particular finding is of significant importance for the design of low-rise buildings and is expected, for very first time, to partially justify the 30% reduction of the effective wind load for the design of the foundation, suggested by the National Building Code of Canada (NBCC 2010, Users Guide - Figure I-7).

## 4 Conclusions

A full-scale facility that includes a low-rise wood building and two weather towers was used to monitor the wind-induced structural response of the test building. Wind, pressure and force data were collected during strong wind events and were used to evaluate how wind-induced forces are transferred from the building envelope to the foundation wall. The field studies were

also supported by detailed wind tunnel simulation and finite element analysis. The wind tunnel simulation was verified in terms of pressure coefficients and force coefficients. The agreement with full scale was particularly good for the case of mean and peak pressure coefficients, especially when a range of wind tunnel wind directions was compared to the field record.

Of particular interest is the field measurement of forces, which were acquired at the truss to wall interface and at the foundation level by several load cells. These forces were compared in terms of correlation plots and reduction factors and the results verified the expected load transfer patterns, showing the highest correlation for the foundation locations immediately below the examined roof load cell. As the load travels farther to the rest of the foundation walls the correlation decreases significantly. Moreover, it was found that irrespective of the wind direction, the majority of the wind uplift force is transferred to the two side walls whereas the end walls have a significantly smaller contribution (less than 30% of the total wind uplift force). The most important finding was related to the structural attenuation which was observed by comparing the numerically derived to the experimentally recorded roof and foundation forces. The comparisons, both in terms of time series and power spectra, verified the statement that wind design practices based on static analysis of structural systems will tend to conservatively estimate true building performances. It was estimated that the reduction of the wind load as it reaches the foundation level is at least 17% and it may reach 28% for certain wind directions.

**Acknowledgements**

The authors acknowledge the support received for this study from the Natural Sciences and Engineering Research Council of Canada through a cooperative research and development grant,

as well as the research discovery grant to the second author. In addition, supports from the Canadian Wood Council and FPInnovations are greatly appreciated.

**References**

Bartlett, F. M., Galsworthy, J. K., Henderson, D., Hong, H. P., Iizumi, E. and Inculet, D. R. 2007. The three little pigs project: A new test facility for full-scale small buildings. 12th International Conference on Wind Engineering, Cairns, Australia. 1623-1630.

Datin, P. L. 2010. Structural load paths in low-rise, wood-framed structures. PhD Thesis, Department of Civil and Coastal Engineering, University of Florida, Gainesville, FL.

Doudak, G. 2005. Field determination and modeling of load paths in wood light-frame structures. PhD Thesis, De-partment of Civil Engineering and Applied Mechanics, McGill University, Montreal, Quebec, Canada.

Eaton K. J. and Mayne J. R. 1975. The measurement of wind pressures on two-storey houses at Aylesbury. Journal of Wind Engineering and Industrial Aerodynamics, 1 (1), 67-109.

Kim, S. I. and Mehta, K. C. 1977. Wind loads on flat roof area through full-scale experiment. Institute for Disaster Research, Texas Tech University, Lubbock, Texas.

Kopp, G. A., Morrison, M. J., Gavanski, E., Henderson, D. J. and Hong, H. P. 2010. "Three little Pigs" Project: Hurricane risk mitigation by integrated wind tunnel and full-scale laboratory tests. Natural Hazards Review, 11 (4), 151-161.

Leatherman, S. P., Gan Chowdhury, A. and Robertson, C. J. 2007. Wall of wind full-scale destructive testing of coastal houses and hurricane damage mitigation. Journal of Coastal Research, 23(5), 1211-1217.

Levitan, M. L. 1988. Statistical analysis to validate full scale wind and structural response data. MSc Thesis, Department of Civil Engineering, Texas Tech University, Lubbock, TX.

Levitan, M. L. and Mehta, K. C. 1992a. Texas Tech field experiments for wind loads part 1: Building and pressure measuring system. Journal of Wind Engineering and Industrial Aerodynamics, 43(1-3), 1565-1576.

Levitan, M. L. and Mehta, K. C. 1992b. Texas Tech field experiments for wind loads part II: Meteorological in-strumentation and terrain parameters. Journal of Wind Engineering and Industrial Aerodynamics, 43(1-3), 1577-1588.

National Building Code of Canada - NBCC 2010. National Research Council of Canada (NRCC), Ottawa, Canada.

Robertson, A. P. and Glass, A. G. 1988. The Silsoe structures building - its design, instrumentation and research facilities. AFRC Inst. Engng. Res., Silsoe, Div. Note DN 1482.

Robertson, A.P., Hoxey, R.P., Short, J.L., Ferguson, W.A. and Blackmore, P.A. 1998. Prediction of structural loads from fluctuating wind pressures: Validation from full-scale force and pressure measurements. Journal of Wind Engineering and Industrial Aerodynamics, 74-76, 631-640.

Zisis, I., and Stathopoulos, T. 2009. Wind-induced cladding and structural loads on a low wooden building. Journal of Structural Engineering, ASCE, 135 (4), 437-447.

Zisis, I., Stathopoulos, T., Smith, I. and Doudak, G. 2011. Cladding pressures and primary structural system forces of a wood building exposed to strong winds. Canadian Journal of Civil Engineering, NRC Research Press, 38, 974-983.

Zisis, I. 2011. Wind load paths on wood buildings. PhD Thesis, Department of Building, Civil and Environmental Engineering, Concordia University, Montreal, Quebec, Canada.

**List of Figure Captions**

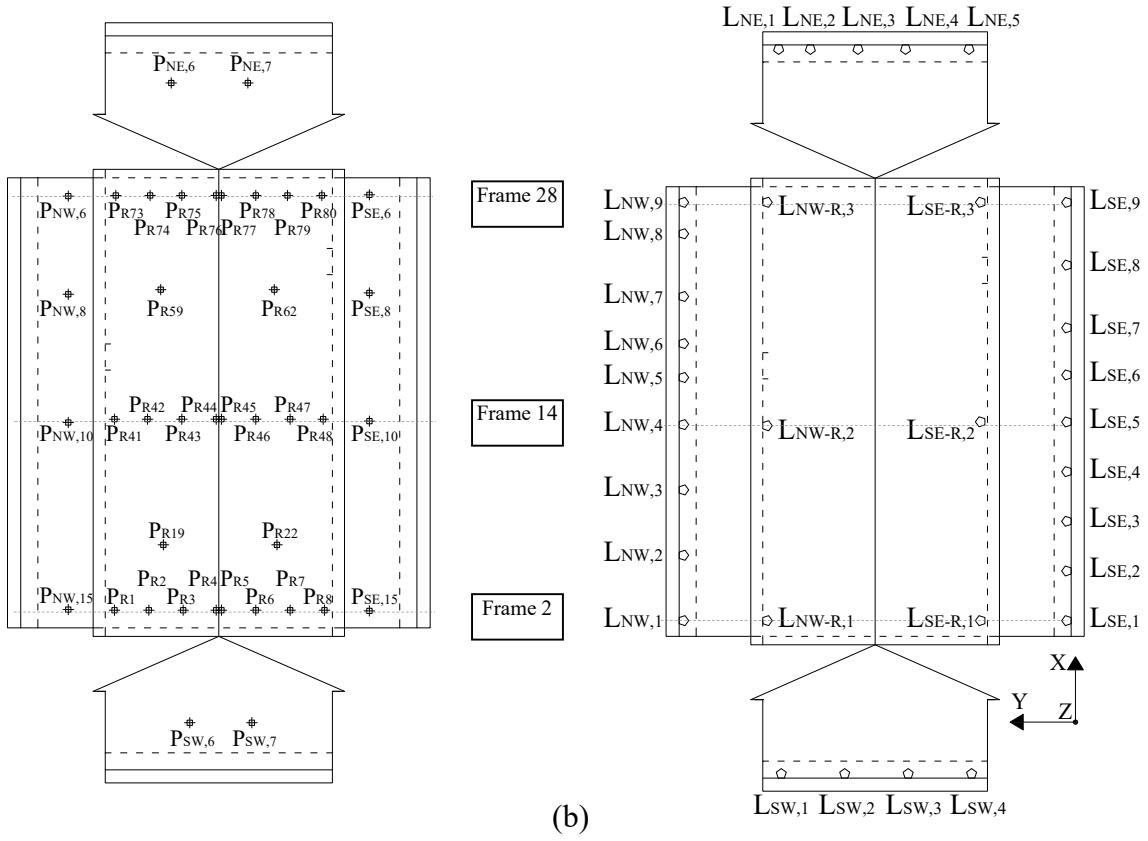


(a) (b)

Figure 1. Pressure tap (a) and load cell (b) location on the test building.

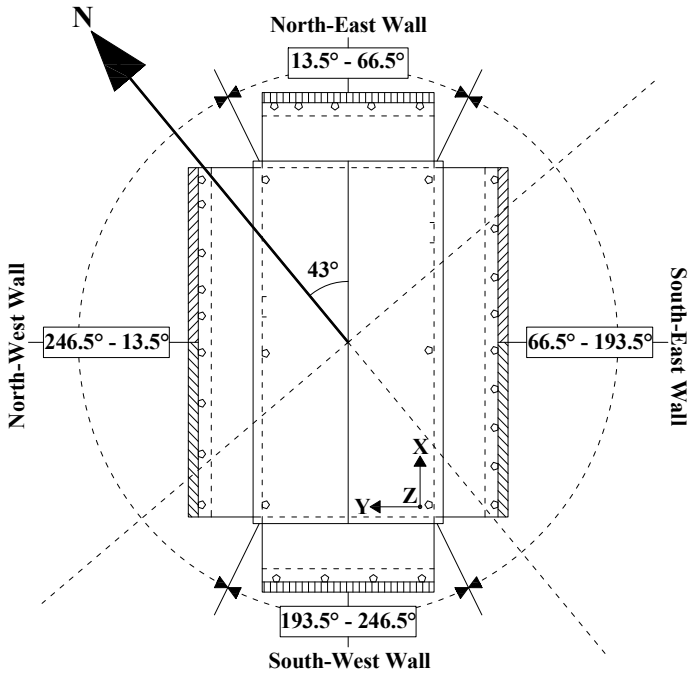


Figure 2. Test house orientation and wall notation.

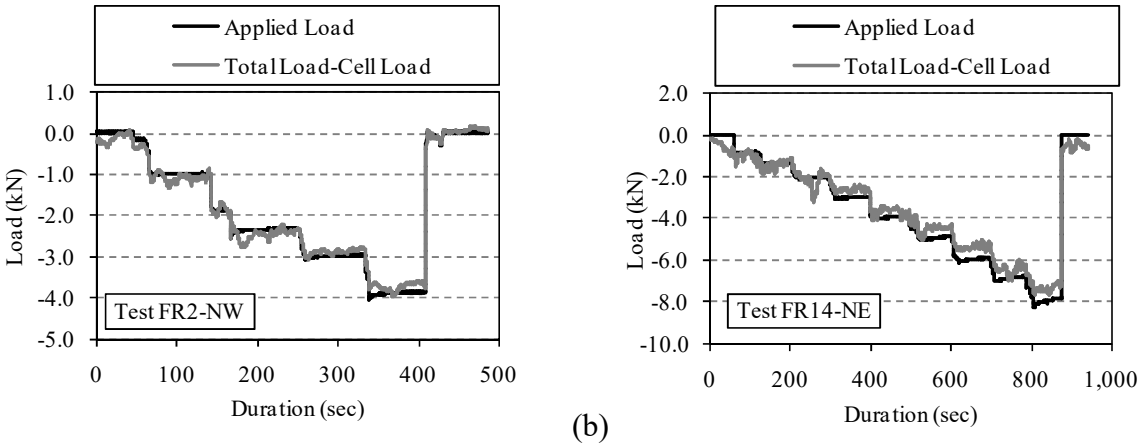


Figure 3. Static load test verification results for FR2-NW and FR14-NW tests.

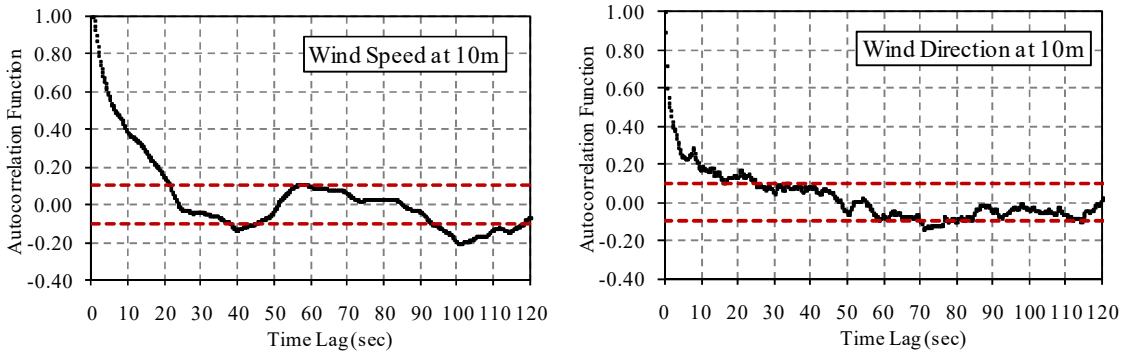


Figure 4. Autocorrelation function of the wind speed and direction at 10 meters height (May 21, 2009).

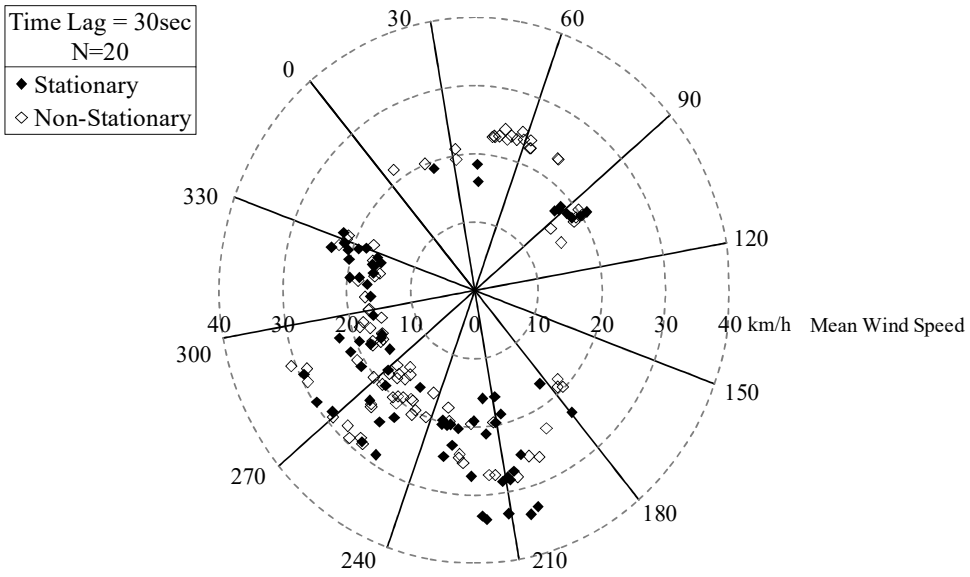


Figure 5. Stationary and non-stationary records of RUN/TREND tests for 30-sec time lag.

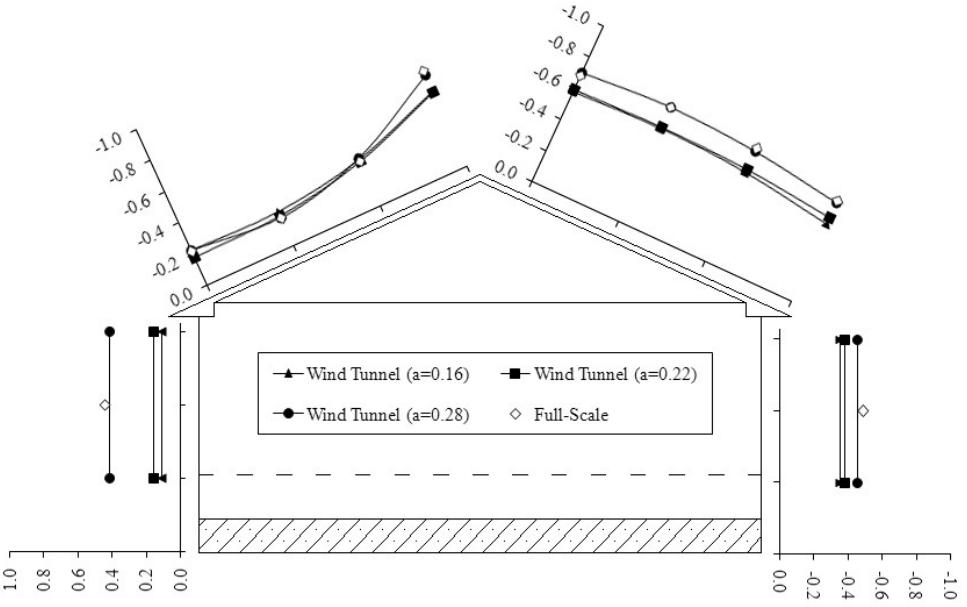


(a)

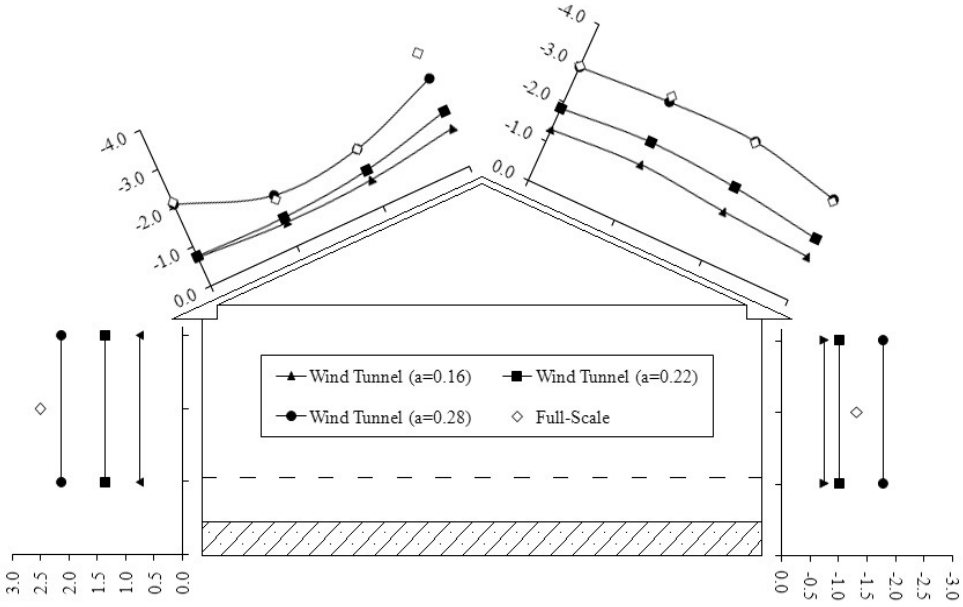


(b)

Figure 6. Mean (a) and peak (b) pressure coefficients for Frame 14 (330 degrees wind direction).

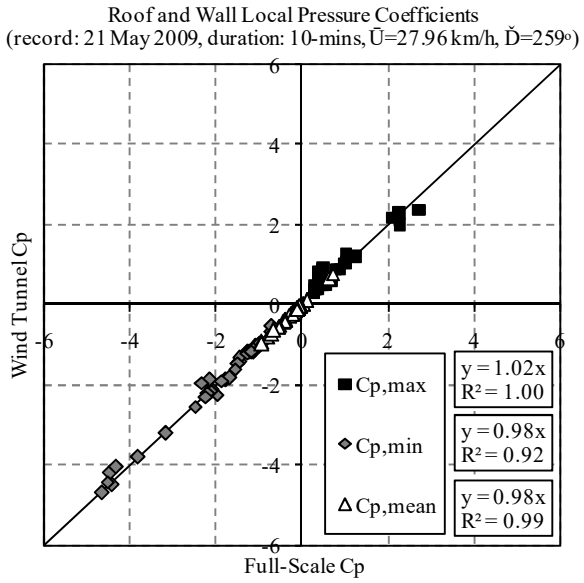


Figure 7. Comparison of wind tunnel and field mean and peak pressure coefficients (21 May, 2009).

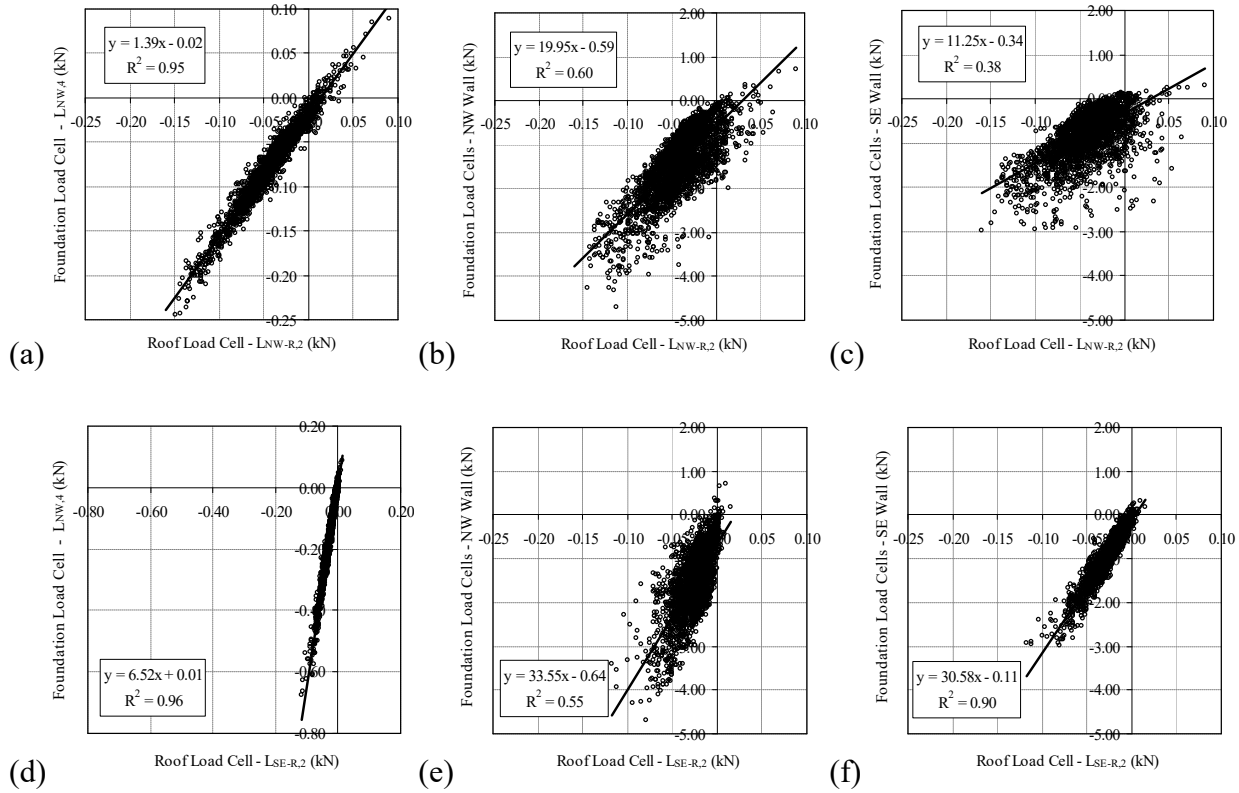


Figure 8. Correlation plots between roof load cell $L_{NW\text{-}R,2}$ (a-c), $L_{SE\text{-}R,2}$ (d-f) and various foundation load cells.

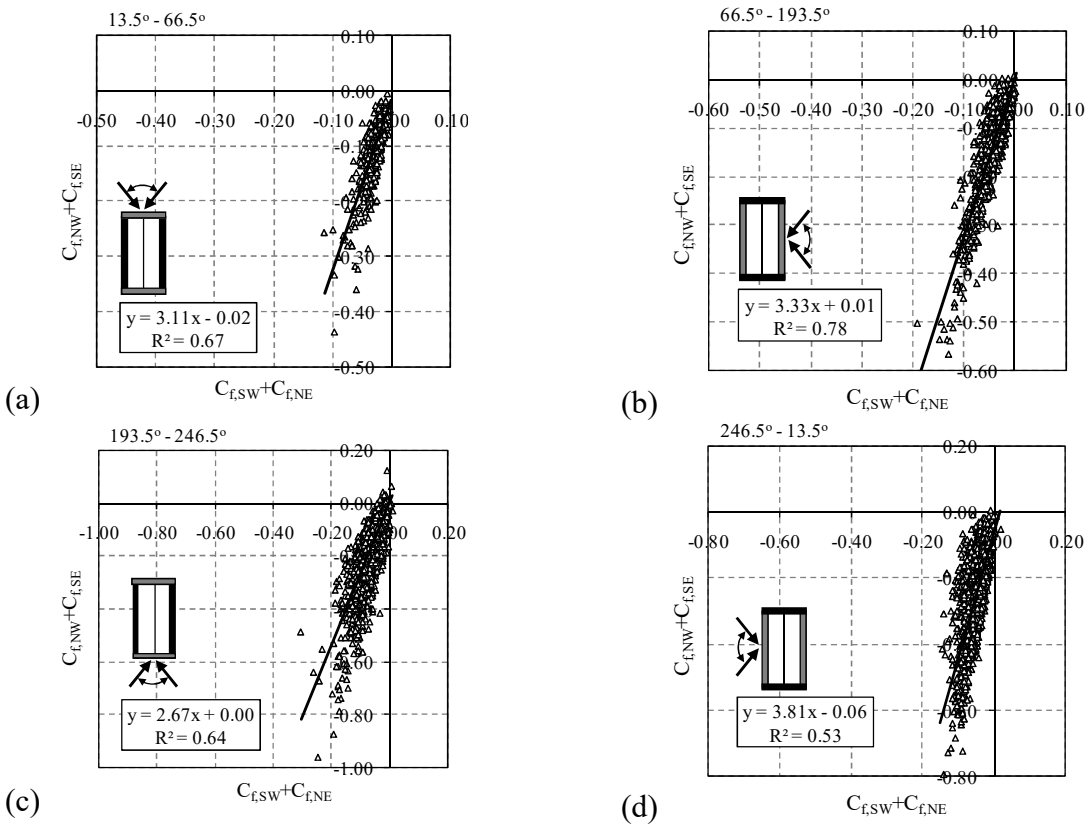


Figure 9. Correlation of sidewall to endwall force coefficients for North-East (a), South-East (b), South-West (c) and North-West (d) incident wind.

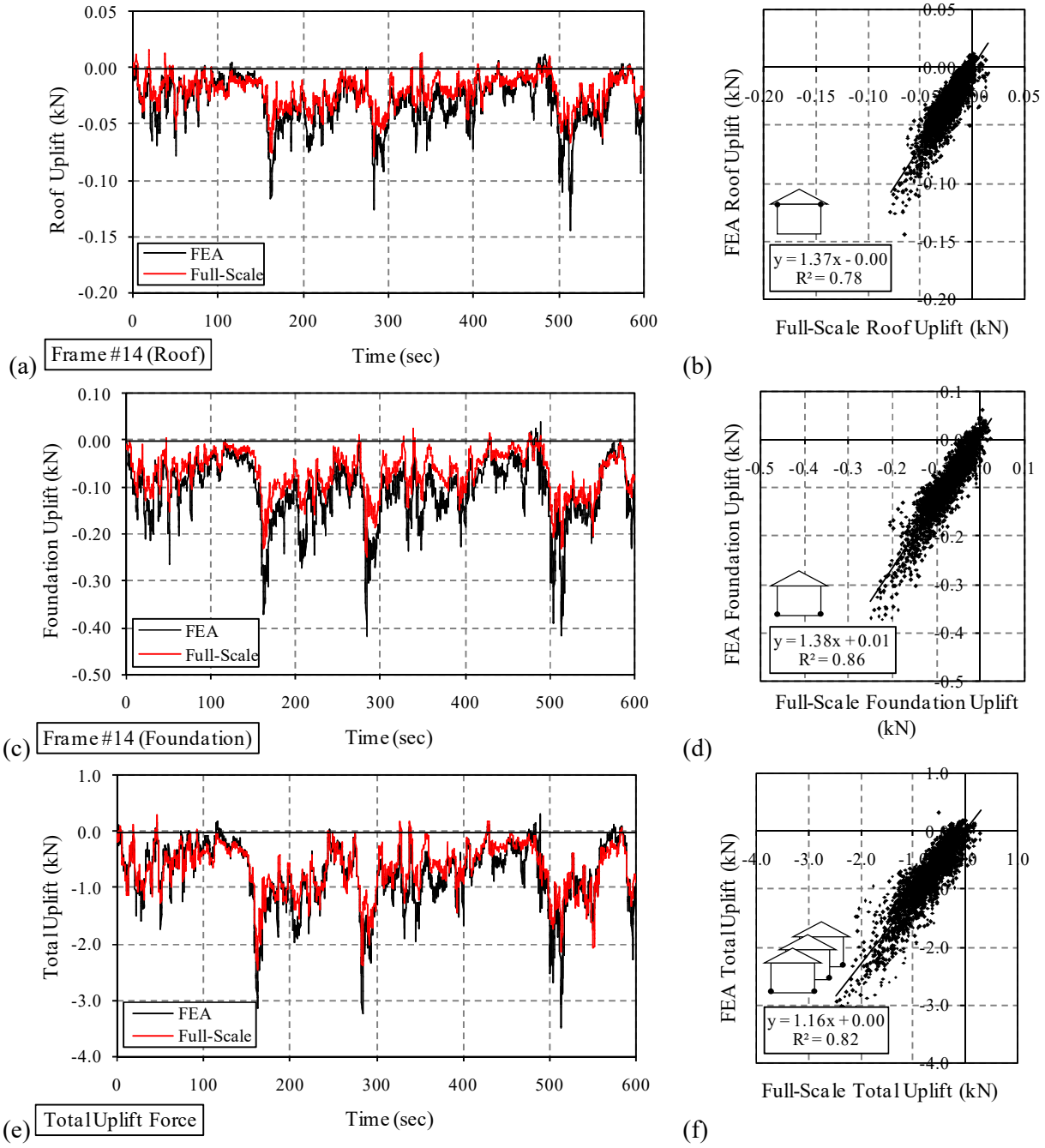


Figure 10. Comparison of load cell and finite element Frame 14 roof uplift forces (a-b), Frame 14 foundation uplift forces (c-d) and total foundation uplift forces (e-f).

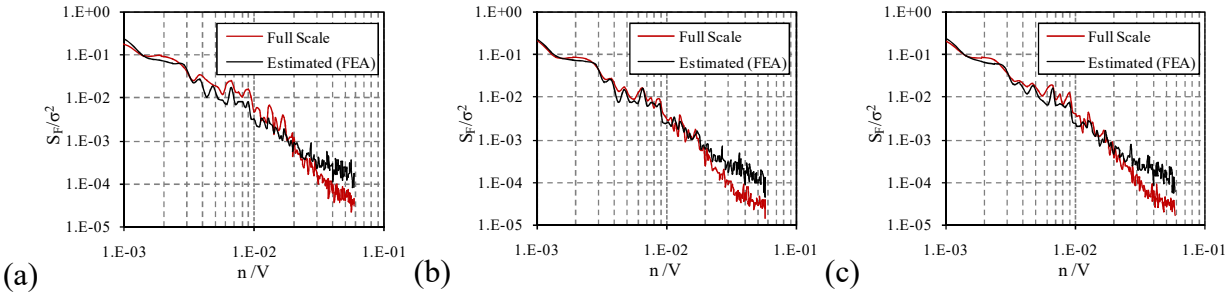


Figure 11. Comparison of numerically derived and experimentally acquired force spectra; roof – one frame (a), foundation - one frame (b), foundation - entire building (c).

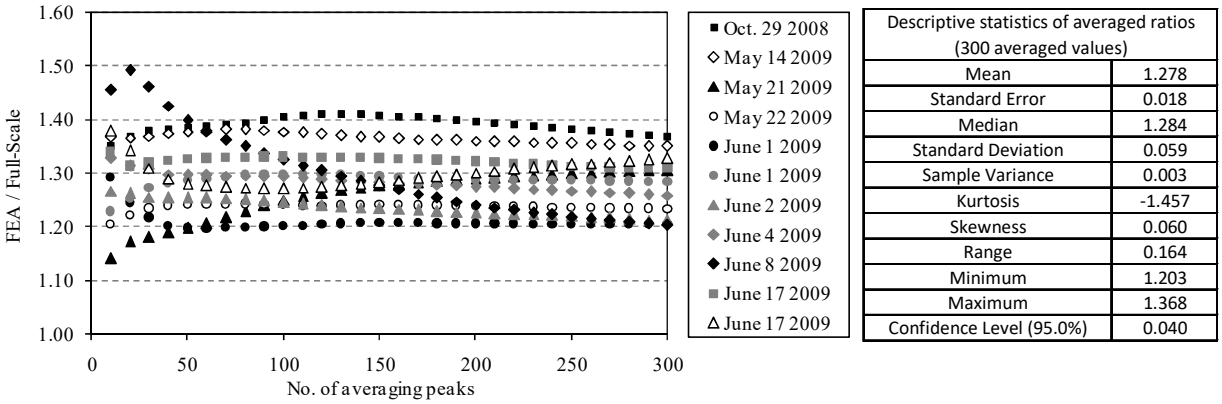


| Descriptive statistics of averaged ratios (300 averaged values) | |
|---|---|
| Mean | 1.278 |
| Standard Error | 0.018 |
| Median | 1.284 |
| Standard Deviation | 0.059 |
| Sample Variance | 0.003 |
| Kurtosis | -1.457 |
| Skewness | 0.060 |
| Range | 0.164 |
| Minimum | 1.203 |
| Maximum | 1.368 |
| Confidence Level (95.0%) | 0.040 |

Figure 12. Finite element to load cell total uplift peak force ratio variation (all foundation load cells).

**List of Table Captions**

Table 1. Wind tunnel experimental values for power law exponent, terrain roughness and turbulence intensity at ridge height.

Table 1. Wind tunnel experimental values for power law exponent, terrain roughness and turbulence intensity at ridge height.

| Terrain | Power Law Exponent ($\alpha$) | Terrain Roughness ($z_0$) - cm | Turbulence Intensity (Ridge Height) - % |
|---|---|---|---|
| Open | 0.16 | 0.012 | 17.9 |
| Light Suburban | 0.22 | 0.069 | 20.2 |
| Heavy Suburban | 0.28 | 0.198 | 26.4 |